International Journal of Nanomedicine

Dovepress
open access to scientific and medical research

Open Access Full Text Article

ORIGINAL RESEARCH

Electrospun PCL/mupirocin and chitosan/lidocaine hydrochloride multifunctional double layer nanofibrous scaffolds for wound dressing applications

This article was published in the following Dove Press journal:
International Journal of Nanomedicine

Xiaoming Li[1]
Chao Wang[2]
Shuang Yang[3]
Ping Liu[1]
Bo Zhang[1]

[1]Department 4, State Key Laboratory of Trauma, Burns and Combined Injury, Institute of Surgery Research, Daping Hospital, Army Medical University, Chongqing 400042, China; [2]Department of Pediatric Intensive Care Unit, Children's Hospital of Chongqing Medical University, Ministry of Education Key Laboratory of Child Development and Disorders, Chongqing 400014, China; [3]Key Laboratory of Biorheological Science and Technology, Research Center of Bioinspired Materials Science and Engineering, College of Bioengineering, Chongqing University, Chongqing 400030, China

Correspondence: Bo Zhang
Department 4, State Key Laboratory of Trauma, Burns and Combined Injury, Institute of Surgery Research, Daping Hospital, Army Medical University, Chongqing 400042, China
Tel +86 23 6875 7443
Email zhangbo67184@163.com

Background: An ideal wound dressing should exhibit good biocompatibility, minimize pain and infection, absorb excess exudates, and maintain a moist environment. However, few clinical products meet all these needs. Therefore, the aim of this study was to fabricate a multifunctional double layer nanofibrous scaffolds (DLS) as a potential material for wound dressing.

Materials and methods: The scaffold was formed from mupirocin and lidocaine hydrochloride homogeneously incorporated into polycaprolactone as the first layer of scaffolds and chitosan as the second layer of scaffolds nanofibers through electrospinning. The fabricated nanofibrous scaffolds were characterized by scanning electron microscopy, Fourier transform infrared spectroscopy, thermogravimetric analysis, differential scanning calorimetry, and measurement of swelling ratio, contact angle, drug release, and mechanical properties. Furthermore, antibacterial assessment, live/dead cell assays, and MTT assays were used to investigate the antibacterial activity and cytotoxicity of the nanofibrous scaffolds.

Results: The morphology of the nanofibrous scaffolds was studied by scanning electron microscopy, showing successful nanofibrous scaffolds. Fourier transform infrared spectroscopy demonstrated the successful incorporation of the material used to produce the produced nanofibrous scaffolds. Thermal studies with thermogravimetric analysis and differential scanning calorimetry indicated that the DLS had high thermal stability. The DLS also showed good in vitro characteristics in terms of improved swelling ratio and contact angle. The mechanical results revealed that the DLS had an improved tensile strength of 3.88 MPa compared with the second layer of scaffold (2.81 MPa). The release of drugs from the scaffold showed different profiles for the two drugs. Lidocaine hydrochloride exhibited an initial burst release (66% release within an hour); however, mupirocin exhibited only a 5% release. Furthermore, the DLS nanofibers displayed highly effective antibacterial activities against *Staphylococcus aureus, Escherichia coli*, and *Pseudomonas aeruginosa* and were nontoxic to fibroblasts.

Conclusion: The fabricated DLS exhibited excellent hydrophilicity, cytocompatibility, sustained drug release, and antibacterial activity, which are favorable qualities for its use as a multifunctional material for wound dressing applications.

Keywords: electrospinning, chitosan, PCL, multifunction, wound dressing, nanofiber

Introduction

The skin is the largest organ in the human body, with an important role in homeostasis and prevention of invasion by microorganisms.[1] Patients suffering from burns, trauma, or other conditions such as diabetic foot ulcers can experience acute soreness

submit your manuscript | www.dovepress.com
Dovepress
http://dx.doi.org/10.2147/IJN.S177256

and serious infections, as well as major medical burdens.[2] Therefore, a wound dressing, as a skin barrier, is essential for wound healing.[3,4] An ideal wound dressing should exhibit good biocompatibility, minimize pain and infection, and facilitate patient compliance and comfort. In addition, dressings should absorb excess exudates and maintain a moist environment on the wound surface.[5–8] Although clinical products exist that can meet these needs, no single dressing addresses all the above issues.[9,10] Therefore, in this work, an antimicrobial agent in a double layer nanofibrous wound dressing was developed and investigated.

Nanofibers can be fabricated using a number of processing techniques, such as emulsion freeze drying,[11] self-assembly,[12,13] and phase separation.[14] However, not all these techniques are ideal for wound dressing fabrication, as the produced nanofibers have large diameters and consequently low porosity.[15] In addition to these manufacturing methods, the electrospinning technique is ideal for wound dressing fabrication, as electrospun nanofibers show large surface area to volume ratios and high porosity with small pores.[16] Additionally, electrospinning is a facile, cost-effective, and versatile technique to fabricate nanofibers from natural and synthetic polymer composites.[17]

Recently, a variety of natural and synthetic polymer composites have been electrospun successfully for wound healing applications. Poly(vinyl alcohol),[18] poly(lactic acid),[15,19] polycaprolactone (PCL),[20,21] and poly(ethylene oxide)[22] are some of the synthetic polymers used for this application. Synthetic polymers have great flexibility in synthesis and modification, but they lack cell-binding sites and biomolecular signatures that can mimic natural tissue.[21,23] Compared with synthetic polymers, natural polymers exhibit low immunogenicity and better biocompatibility and can mimic the native extracellular matrix (ECM) of biological tissue.[14,21,24] Widely used natural polymers for wound healing include chitosan,[1,16] collagen,[25,26] alginate,[27] gelatin,[28] chitin,[29] and silk fibroin.[30] However, wound dressings prepared from natural polymers are unable to retain their structural stability,[31] while those from synthetic polymers usually have good mechanical properties.[14,21] Interestingly, a nanofibrous scaffold achieved by combining natural and synthetic polymers is expected to exhibit physicochemical properties of both components.[16,24]

Chitosan, the most important derivative of chitin, has been extensively studied for biomedical applications owing to its highly porous structure, biocompatibility, and intrinsic antibacterial nature.[32,33] Furthermore, composites of chitosan have been proven to enhance tissue regeneration. Previous studies showed that chitosan nanofibrous scaffolds could be applied as a biomimetic ECM to support the proliferation of smooth muscle cells, neural cells, and fibroblasts.[16,32,34] However, chitosan alone cannot be used for this purpose, owing to its poor mechanical properties.[35] Hence, to obtain nanofibrous scaffolds, chitosan must be combined with synthetic electrospun polymers such as PCL. PCL has been widely used as a synthetic polymer owing to its excellent electrospinnability and favorable mechanical properties.[8,36,37]

There are several reports in the literature of efforts to produce multifunctional wound dressings. For example, some researchers developed multifunctional and biomimetic fish Col/BG nanofibers, which had the ability to induce skin regeneration with adequate tensile strength and contained a certain degree of antibacterial activity against *Staphylococcus aureus*. The Col/BG nanofibers not only had high effective surface area, good water absorbability, and the ability to absorb wound exudates efficiently but the porous structure and small pore size of the electrospun nanofibers could also meet the requirement for high gas permeation and protect the wound from bacterial infection.[38] Furthermore, other researchers have fabricated multifunctional wound dressings based on electrospun fibers, which were capable of achieving wound debridement and wound healing simultaneously as well as multidrug loading suitable for various stages of the healing process.[14]

In this study, the main objective was to fabricate and characterize a chitosan/PCL double layer nanofibrous scaffold for multifunctional wound dressing applications. Initially, chitosan/PCL was blended with lidocaine hydrochloride (LID)/mupirocin and successfully fabricated into a double layer nanofibrous scaffolds (DLS) using an electrospinning technique. The first layer of scaffolds (FLS), which was exposed to the environment, consisted of PCL with the addition of mupirocin to impart antimicrobial activity to the developed wound dressing. The second layer of scaffolds (SLS), which had indirect contact with the wound site, was composed of electrospun chitosan nanofibers incorporated with LID as a model pain-relieving compound. Then, the physical–chemical properties (morphology, porosity, pore size, Fourier transform infrared [FTIR] spectra, water uptake, contact angle, thermal stability, tensile strength, and drug release) were comprehensively analyzed. The nanofibrous scaffolds were also evaluated for their cytocompatibility using human dermal fibroblasts in vitro. Finally, the antibacterial activity of the nanofibrous scaffolds was studied on *S. aureus, Escherichia coli*, and *Pseudomonas aeruginosa*.

Materials and methods

Materials

Chitosan (medium molecular weight), PCL, PBS solution, and MTT were purchased from Sigma-Aldrich Co., St Louis, MO, USA. Trifluoroacetic acid (TFA), LID, and mupirocin were purchased from Sangon Biotech, Shanghai, China. Dichloromethane (DCM) and hexafluoroisopropanol (HFIP) were purchased from Aladdin Reagent Co., Ltd, Shanghai, China. DMEM and penicillin–streptomycin were purchased from HyClone, Logan, UT, USA. The live/dead viability/cytotoxicity assay kit, FBS, and Luria–Bertani (LB) medium were purchased from Thermo Fisher Scientific, Waltham, MA, USA.

Human dermal fibroblasts were obtained from the Department of Dermatology, Daping Hospital, Army Medical University, Chongqing, China. The Ethics Committee of Army Medical University approved the study, and all experiments were performed in accordance with relevant guidelines and regulations (2017-28). All the patients whose tissue samples were used had provided written informed consent. Bacterial strains of *S. aureus* (ATCC 29213), *E. coli* (ATCC 25922), and *P. aeruginosa* (ATCC 27853) were obtained from the Department of Laboratory Medicine, Daping Hospital, Army Medical University, Chongqing, China.

Preparation of electrospinning solutions

FLS

Five hundred milligrams of PCL was dissolved in 5 mL HFIP/DCM at a volume ratio of 1:3 by magnetic stirring for 24 hours at room temperature to obtain a homogeneous solution of concentration 10% (w/v). Subsequently, mupirocin was slowly added to the PCL solution at a ratio of 2% (w/v), under rigorous stirring for 24 hours.

SLS

Initially, 5 mL chitosan solution (8% w/v) was prepared by dissolving the required amount of polymer in 30% DCM and 70% TFA, with magnetic stirring for 48 hours at room temperature to obtain a homogeneous solution. Subsequently, LID was slowly added to the chitosan solution at a ratio of 1% (w/v), with stirring at room temperature until a clear solution was formed.

Electrospinning

The electrospinning setup used in this study consisted of three major components: a high-voltage power supply that could generate a voltage of up to 30 kV (Dongwen High-Voltage Power Supply Plant, Tianjin, China), a 10 mL syringe with a metallic needle of 0.25 mm inner diameter that could control the flow rate of a syringe pump (Longer Precision Pump, Baoding, China), and a collector made from aluminum foil for fiber collection. In the electrospinning process, the FLS, containing PCL/mupirocin, was followed by the deposition of LID-loaded chitosan in the SLS. The detailed parameters are listed in Table 1. All electrospinning experiments were performed at room temperature and a relative humidity of 30%–40%. The obtained PCL/mupirocin, chitosan/LID, and DLS scaffold dressings were labeled as FLS, SLS, and DLS, respectively. The prepared fibrous scaffolds were dried in a vacuum oven for 1 week at room temperature to remove residual solvent before subsequent use.

Characterization of nanofibrous scaffolds

The fiber diameter and the morphology of the electrospun scaffolds were studied using a Zeiss scanning electron microscopy (SEM, Crossbeam 340) unit. Before imaging, the nanofiber samples were sputter coated with gold, and the micrographs were captured at magnifications of 1,000×, 3,000×, and 10,000×. The diameter size distribution in the fabricated membranes was determined using the ImageJ (National Institutes of Health, Bethesda, MD, USA) software, by measuring at least 100 individual fibers randomly. A histogram illustrating the diameter distribution was

Table 1 Parameters for the electrospinning of drug–polymer solutions

Sample	Solvent	Concentration w/v%	Voltage (kV)	Flow rate (mL/h)	Distance (cm)	Needle gauge	Rotation (RPM)
SLS	TFA/DCM 7:3	Chitosan/LID 8:1	17	1	13	25G	150
FLS	HFIP/DCM 1:3	PCL/mupirocin 10:2	15	1	15	25G	150

Abbreviations: DCM, dichloromethane; FLS, first layer of scaffolds; HFIP, hexafluoroisopropanol; LID, lidocaine hydrochloride; PCL, polycaprolactone; SLS, second layer of scaffolds; TFA, trifluoroacetic acid.

also generated using the OriginPro 9 software (OriginLab Corporation, Northampton, MA, USA).

The mechanical characterizations were performed using an ElectroForce 3330 (Bose, Framingham, MA, USA) according to method ASTMD 882-02. Before testing, the cuboid-like shape scaffolds (6,010×0.2 mm^2) were conditioned for 48 hours at 50%±3% relative humidity and 25°C±2°C. The initial distance of separation and loading velocity were fixed at 35 mm and 0.2 mm/s, respectively.

Chemical analyses of the FLS, SLS, and DLS were performed by FTIR spectroscopy over a range of 4,000–400 cm^{-1}. FTIR spectra of different samples were obtained by a Nicolet spectrometer (System 2000, PerkinElmer, Waltham, MA, USA) with a DTGS KBr detector. Approximately 1 mg of dried sample was mixed with 100–120 mg of KBr and compressed into pellets.

The thermal stability of the FLS, SLS, and DLS were studied using a PerkinElmer thermogravimetric analysis (TGA) 4,000 unit (PerkinElmer). Samples of total mass 4 mg were placed in an aluminum pan, and the experiment was carried out under a dry nitrogen atmosphere in the temperature range 30°C–600°C at an ascending rate of 10°C/min. The remaining weight of the sample was recorded at each temperature point, and the values were exported in an Excel sheet. Thermal properties of the FLS, SLS, and DLS were studied using differential scanning calorimetry (DSC; Q20, TA Instruments, New Castle, DE, USA). Five milligrams of each sample was heated up to 120°C at a rate of 10°C/min in the presence of nitrogen as an inert carrier gas flowing at a rate of 25 mL/min.

Water contact angle measurements

The contact angles for a drop of distilled water on electrospun membranes were measured using a contact angle instrument (Future Scientific Ltd. Co., Taiwan, China) at room temperature. A single drop of 5 µL deionized water was dropped on the surface of a flat 10×10 mm^2 membrane using a syringe perpendicular to the surface, and an image was captured less than 1 second after the water droplet became stable on the surface. This process was repeated six times on each membrane. The contact angles were analyzed using software supplied by the manufacturer.

Porosity and pore size

The porosity of the prepared nanofibrous scaffolds was determined using a previously reported method.[1] Briefly, the scaffolds were immersed in absolute ethanol until it was saturated. The scaffolds were weighed before and after the immersion in alcohol. The porosity was calculated using the equation:

$$P = \frac{W_2 - W_1}{\rho V_1} \times 100\%$$

where W_1 and W_2 indicate the weights of the scaffolds before and after immersion in alcohol, respectively; V_1 is the volume before immersion in alcohol; and ρ is a constant (the density of alcohol). All samples were tested in triplicate.

Moreover, the pore size and porosity distribution of the nanofibrous scaffolds were measured using ImageJ, and a graphical representation of pore size distribution was prepared using OriginPro 9.

Swelling ratio of nanofibrous scaffolds

Nanofibrous scaffolds were cut into small pieces of equal weight and immersed in PBS (pH 7.4, 37°C) for 24 hours. Water that adhered to the surface was removed by gently blotting with filter paper, and the scaffolds were immediately weighed.

$$DS = \frac{W_w - W_d}{W_d} \times 100\%$$

In this equation, DS is the degree of swelling, and W_w and W_d represent the wet and dry weights of the scaffolds, respectively. All measurements were performed in triplicate.

Cell culture, MTT, and live/dead cell assays

Human dermal fibroblasts were cultured in DMEM supplemented with 10% (v/v) FBS, 100 U penicillin/mL, and 100 µg streptomycin/mL in a humidified atmosphere of 5% CO_2 and 95% air at 37°C. The cell culture medium was replaced every 3 days. Subculture was performed by digestion with 0.25% trypsin/0.02% EDTA when the cells were nearly confluent and the fourth to eighth passage fibroblasts were used for the seeding.

Human dermal fibroblasts were used to study cell viability on the scaffolds using the MTT assay. Nanofibrous scaffolds were punched (0.6 cm in diameter) and placed in sterile 96-well plates; 200 µL samples of a cell suspension of 1×10^5 count were planted along with each type of scaffold individually per well. After incubation, 0.2 mL of 5 mg/mL MTT was added to the surface of scaffolds, and incubation was continued for another 4 hours. Then, 1 mL of DMSO was added to each well and further incubated for 10 minutes.

The cell viability was determined by measuring the absorbance at 490 nm on a microplate reader (BioTek, Winooski, VT, USA). Cells without scaffolds served as a control. All the experiments were performed in triplicate.

Cell viability was assessed by live/dead staining at 24 hours. According to the manufacturer's protocol, samples were washed with PBS and stained with 100 µL of a solution of 2 µM calcein-AM and 4 µM propidium iodide in PBS. After 15 minutes of incubation at 37°C, the scaffolds with the fluorescently stained cells were viewed under a fluorescence microscope (Olympus Corporation, Tokyo, Japan).

Drug release

The nanofibrous scaffolds were incubated in 20 mL of PBS at 37°C. At predetermined time intervals, 1 mL PBS was collected for testing and replaced with 1 mL of fresh PBS. The amount of drug released from the scaffolds was determined via ultraviolet spectrometry (NanoDrop 2000 spectrophotometer, Thermo Fisher Scientific) at 263 nm (LID) and 218 nm (mupirocin). Serial dilutions of the drugs were measured to obtain standard curves used to calculate the amount of drug released from scaffolds. LID release was linear between 1 and 10 mg/mL ($y = 0.1235x + 0.0308$, $R^2 = 0.9955$), and mupirocin release was linear between 1 and 15 mg/mL ($y = 0.9606x + 0.1445$, $R^2 = 0.9984$).

Antibacterial activity

Drug-sensitive strains of *S. aureus*, *E. coli*, and *P. aeruginosa* were used to evaluate the antibacterial activity of the scaffolds by an inhibition zone method. First, 100 µL of 10^8 CFU/mL bacteria suspension was spread on an LB agar plate, then a scaffold sample with a diameter of 0.9 cm was placed on the surface of the agar. After 24 hours incubation at 37°C, the diameter of the inhibition zone was measured.

Statistical analysis

The data are represented as mean±SD. The statistical analyses to compare the results between two groups were conducted using the paired Student's *t*-test, and a value of $P<0.05$ was considered statistically significant.

Results and discussion

Morphology and diameter distribution

The morphology and nanofiber diameter distributions for the FLS, SLS, and DLS are presented in Figure 1. The structure of SLS consisted of randomly oriented uniform and homogeneous fibers (Figure 1A and B), whereas FLS exhibited a nonhomogeneous structure (Figure 1D and E). Figure 1G–I presents the surface and cross-section SEM photographs of the DLS. It can be seen that both the surface and the interior of the DLS exhibited a double layer nanofiber structure. Moreover, the contact between SLS and FLS was observed to be excellent on the surface and in the interior of the DLS. From the SEM images, the fiber diameters were calculated as the mean value of 100 measurements at various locations. The mean fiber diameter obtained for the SLS was 735±152 nm (Figure 1C), while in the case of the FLS it was 1,031±227 nm (Figure 1F). The diameters of nanofibers were distributed in the range 420–1,390 nm in SLS and 440–1,580 nm in the FLS; this difference in fiber diameters was likely due to the method of preparation. It should be noted that in electrospinning, the fiber diameter is influenced by the distance between syringe and collector, the electric field, and the flow rate properties of the solution (conductivity, concentration, and viscosity).[21] SLS fibers showed smaller diameters than FLS fibers, likely owing to the lower concentration of the SLS solution. Typically, when the concentration is increased, the diameter increases proportionally.[39]

Mechanical properties

The mechanical properties (peak load, tensile strength, Young's modulus, and elongation at break) of the FLS, SLS, and DLS are summarized in Table 2. PCL scaffolds are known to be highly flexible and elastic,[14] whereas chitosan scaffolds have been reported to be brittle and weak.[35,40] Higher peak load values were observed for both the FLS (7.57 N) and the DLS (4.31 N) than for the native polymer scaffolds (SLS, 3.12 N). The tensile strengths of the DLS (3.88 MPa) and FLS (6.82 MPa) were significantly increased in comparison with SLS (2.81 MPa), although the SLS scaffolds possessed a tensile strength of 2.81 MPa, which is higher than that of the reported lyophilized chitosan dressing (0.48 MPa).[1] The elongation at break values (FLS, 68.31%; DLS, 14.93%) were also greater than those of the native polymers (SLS, 12.37%). Moreover, the Young's moduli of the SLS, FLS, and DLS were 37.98, 2.99, and 25.47 MPa, respectively. Therefore, the DLS showed intermediate tensile properties between those observed for FLS and SLS. All these observations of mechanical properties suggest that a nanofibrous scaffold combining natural and synthetic polymers can demonstrate appreciable mechanical strength compared with natural polymer scaffolds similar to the observations made by Fu et al.[36]

Porosity and pore size

The porosity and pore size distribution of the scaffolds are shown in Figure 2. SLS had a porosity of 74% of the total

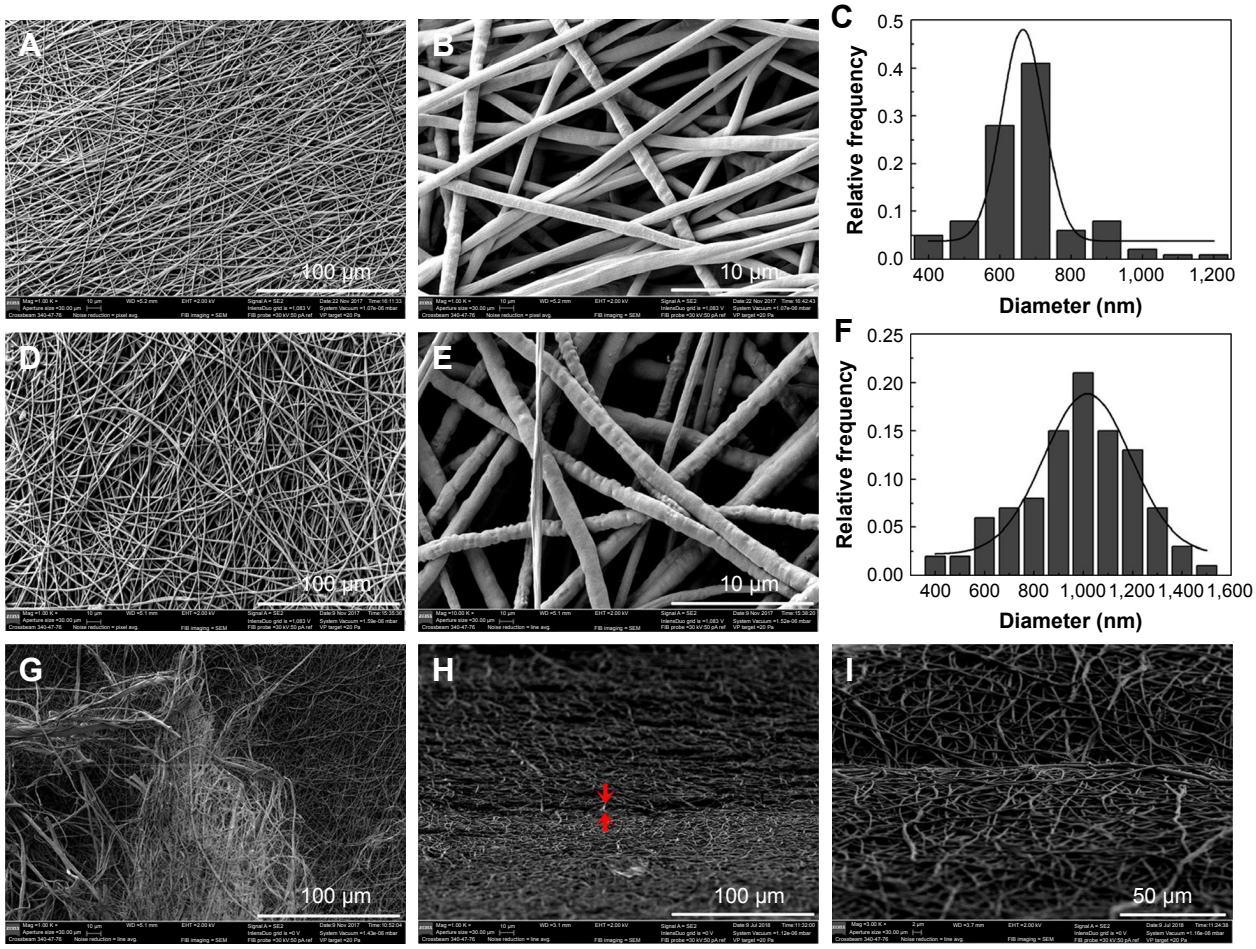

Figure 1 Nanofiber morphology and diameter distribution of fabricated nanofibrous scaffolds.
Notes: Representative SEM images of SLS (**A**, **B**), FLS (**D**, **E**), and DLS (**G**–**I**). The surface morphologies were observed and photographed at 1,000× (**A**, **D**, **G**) and 10,000× (**B**, **E**). The fracture surface morphologies were observed and photographed at 1,000× (**H**) and 3,000× (**I**). Diameter distribution histogram of SLS (**C**) and FLS (**F**) nanofibrous scaffolds.
Abbreviations: DLS, double layer nanofibrous scaffolds; FLS, first layer of scaffolds; SEM, scanning electron microscopy; SLS, second layer of scaffolds.

scaffold volume (Figure 2A), and there was a significant difference compared with FLS (86%). However, with the addition of SLS to the FLS sample, the porosity decreased to 71%–86%, slightly higher than that reported for cationic chitosan-graft-poly(ε-caprolactone)/PCL (40/60) hybrid scaffolds (77%).[37] Compared with other methods, scaffolds produced by electrospinning have higher porosity. For example, a chitosan sponge prepared by a lyophilization process showed porosity in the range of 63%–68%.[1] The high porosity of the scaffolds is beneficial in a wound dressing not only to promote moisture and prevent infection but also for the transfer of nutrients and oxygen exchange.[2,31]

In SLS, the pore size was distributed between 1 and 7 μm with a mean value of 4.19±1.02 μm. FLS exhibited a minor increase in mean pore size (7.05±1.87 μm), and the distribution fell in the range 3–11 μm as illustrated in Figure 2B and C. However, when comparing the pore size with that determined by SEM of lyophilized chitosan, an increased pore size (20–100 μm) was observed in the AgNPs/chitosan dressing.[1] Furthermore, the pore size distribution was narrow and sharp for SLS and became broader for FLS with increasing fiber diameters. Scaffolds with smaller fiber diameters have been widely reported to have smaller pore sizes and narrower pore size distributions.[20,37,41]

Table 2 Mechanical properties of scaffolds

Sample	Peak load F_b/N	Tensile strength σ_b/MPa	Young's modulus E/MPa	Elongation at break δ/%
SLS	3.12	2.81	37.98	12.37
FLS	7.57	6.82	2.99	68.31
DLS	4.31	3.88	25.47	14.93

Abbreviations: DLS, double layer nanofibrous scaffolds; FLS, first layer of scaffolds; SLS, second layer of scaffolds.

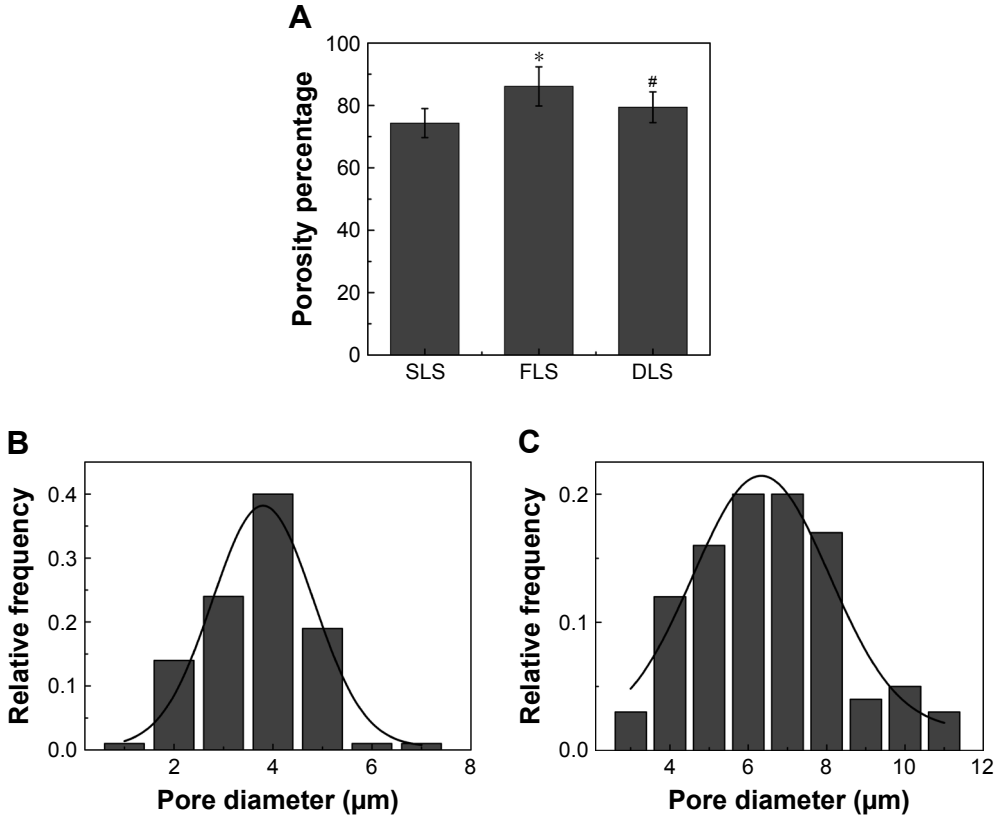

Figure 2 Porosity and pore size distribution of the nanofibrous scaffolds.
Notes: Porosity percentage (**A**). Pore size distribution of SLS (**B**) and FLS (**C**). *The difference in mean is significant ($P<0.05$) with respect to chitosan. #The difference in mean is significant ($P<0.05$) with respect to PCL.
Abbreviations: DLS, double layer nanofibrous scaffolds; FLS, first layer of scaffolds; PCL, polycaprolactone; SLS, second layer of scaffolds.

FTIR

FTIR spectroscopy was used to assess the physical and chemical interaction of the polymers.[25] Figure 3 shows the FTIR spectra of LID, chitosan, SLS, mupirocin, PCL, FLS, and DLS. As shown in Figure 3A, LID showed two characteristic bands around 3,385 and 1,686 cm^{-1} that could be attributed to N–H stretching and C=O stretching.[42] In the spectrum of chitosan (Figure 3B), the characteristic bands of saccharine appeared 889 and 1,147 cm^{-1}. The absorbances of amide I, II, and III bands in chitosan were observed at 1,653, 1,420, and 1,320 cm^{-1}, respectively. In addition, the spectra showed characteristic absorption peaks at around 1,071 and 1,155 cm^{-1}, which were assigned to the C–O stretching vibration. On the contrary, the spectrum of chitosan demonstrated two characteristic bands at 3,369 and 2,874 cm^{-1}, attributed to amine N–H symmetrical vibration and the typical C–H.[16,37] These characteristic bands were also observed in the spectra of LID and chitosan physical mixtures (Figure 3C), indicating the absence of chemical interactions between chitosan and LID during the manufacturing process.

The FTIR spectrum of mupirocin (Figure 3D) showed characteristic bands at 1,712 cm^{-1} corresponding to C=O stretching, at 2,859 and 2,929 cm^{-1} corresponding to C–H deformation, at 1,150 cm^{-1} corresponding to the C–O–C stretching vibration, and at 1,052 cm^{-1} corresponding to the C–C skeleton.[43] PCL (Figure 3E) showed a strong characteristic band at 1,734 cm^{-1} corresponding to C=O stretching and two bands at 2,859 and 2,929 cm^{-1} due to $-CH_2$ group stretching.[45] The FTIR spectra of FLS (Figure 3F) exhibited absorbance bands at 1,150, 1,052, and 1,734 cm^{-1}, which were assigned to the characteristic bands of C–O–C in mupirocin, the C–C skeleton, and C=O in PCL, respectively. This indicates that mupirocin was successfully grafted onto PCL. The FLS and SLS characteristic bands were also observed in the spectrum of the DLS (Figure 3G), indicating the absence of chemical interactions between FLS and SLS during the manufacturing process.

Thermal stability

Following FTIR analysis, DSC and TGA were used to further explore the interactions between the drug and the polymer

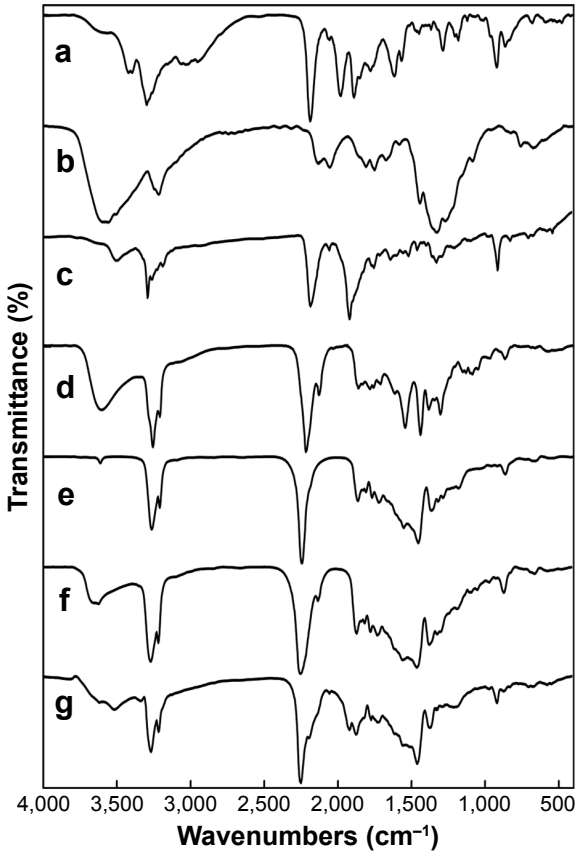

Figure 3 FTIR spectrum of LID (**a**), chitosan (**b**), SLS (**c**), mupirocin (**d**), PCL (**e**), FLS (**f**), and DLS (**g**).
Abbreviations: DLS, double layer nanofibrous scaffolds; FLS, first layer of scaffolds; FTIR, Fourier transform infrared spectra; LID, lidocaine hydrochloride; PCL, polycaprolactone; SLS, second layer of scaffolds.

within the polymeric matrix. The recorded TGA and DSC curves are shown in Figure 4. SLS had three distinct weight loss stages. The first occurring at about 40°C was ascribed to the vaporization of bound water. The second stage of weight loss began at 130°C and was related to the thermal decomposition of LID. In the third stage, the weight loss at about 250°C was primarily attributed to the decomposition of chitosan. Notably, SLS showed increased weight loss compared with chitosan, which could be attributed to the fact that LID decomposes to a greater degree than chitosan under the same conditions. It could also be inferred from the TGA curves that the FLS and DLS underwent three stages of weight loss owing to the loss of absorbed water and the thermal decomposition of the polymer.

The DSC thermograms of chitosan, PCL, SLS, FLS, and DLS are shown in Figure 4B. The endothermic peak occurred at 50°C for chitosan, whereas it shifted slightly to 51°C for SLS composites. For PCL, an endothermic peak at 58°C was observed, while for the FLS and DLS it was observed at 63°C; this shift could be attributed to the chemical linkage between mupirocin and PCL, resulting in a higher endothermic peak. The higher endothermic peak suggests that the DLS has high stability in high-temperature environments.[44]

Contact angles and swelling ratio

Wettability is a major criterion for a wound dressing material, as it affects cell adhesion, proliferation, and the ability to absorb exudates.[1,36] The water contact angle can be used to evaluate wettability. Water contact angles of the FLS, SLS, and DLS are shown in Figure 5A. The average contact angles of the SLS (24.9°±2.5°), FLS (56.3°±2.3°), and DLS (34.6°±4.6°) reflect the hydrophobic behavior of the FLS as well as the role of the SLS in bestowing hydrophilicity on the DLS. Moreover, the SLS was highly hydrophilic with a contact angle of 24.9° owing to the presence of hydrophilic amino groups and hydroxyl groups on its surface.[37]

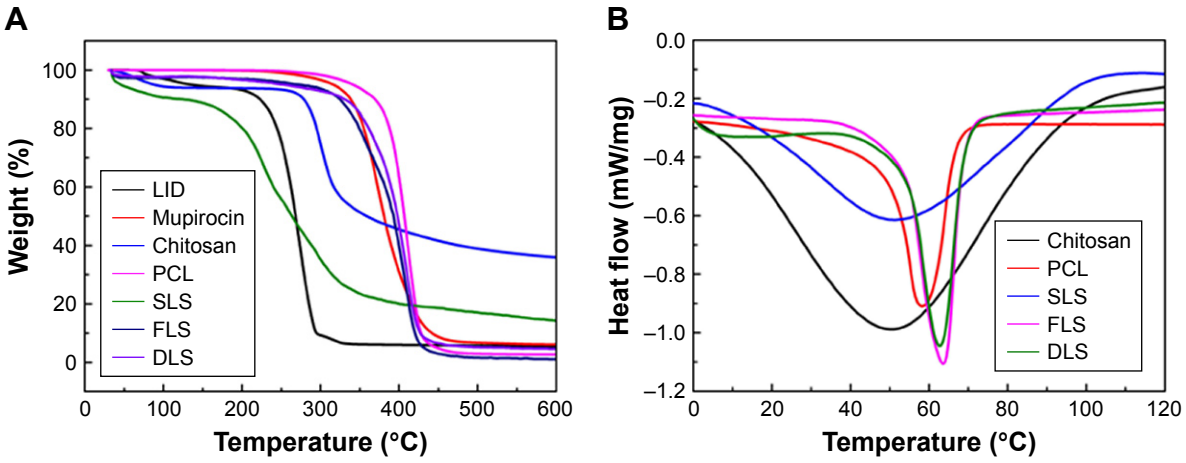

Figure 4 Thermal stability of chitosan and PCL nanofibrous scaffolds.
Notes: TGA graph (**A**) and DSC graph (**B**).
Abbreviations: DLS, double layer nanofibrous scaffolds; DSC, differential scanning calorimetry; FLS, first layer of scaffolds; LID, lidocaine hydrochloride; PCL, polycaprolactone; SLS, second layer of scaffolds; TGA, thermogravimetric analysis.

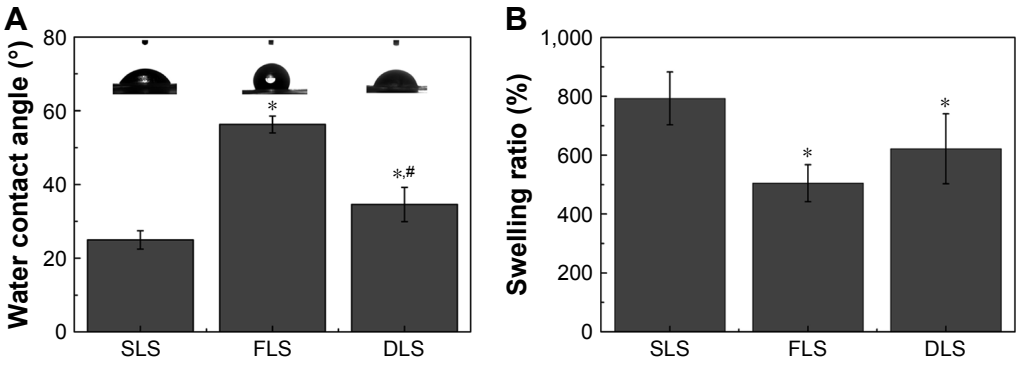

Figure 5 Water contact angles and swelling ratio of nanofibrous scaffolds.
Notes: Water contact angles of nanofibrous scaffolds (**A**). Swelling ratio of nanofibrous scaffolds (**B**). *The difference in mean is significant ($P<0.05$) with respect to SLS. #The difference in mean is significant ($P<0.05$) with respect to FLS.
Abbreviations: DLS, double layer nanofibrous scaffolds; FLS, first layer of scaffolds; SLS, second layer of scaffolds.

The swelling ratio is another criterion that can be used to assess wound dressings.[31,45] Figure 5B shows the swelling behaviors of the FLS, SLS, and DLS in PBS. All the scaffolds possessed a high swelling capacity after saturation with PBS. Swelling ratio analysis revealed that the SLS had a swelling ratio of 793%, while the DLS showed a lower swelling ratio of about 622%. The reduced swelling ratio could be attributed to the reduction of hydrophilic groups in the FLS (505%). This observation is in agreement with the water contact angle study, in which the SLS had a decreased contact angle when in composite with the FLS. The highly hydrophilic and good swelling property of the DLS enables it to absorb exudates at the wound site to maintain a moist environment.[1]

Cytotoxicity test

In order to differentiate live/dead cells from fibroblasts, we used the live/dead cell assay, in which green fluorescence is observed in live cells, while dead cells show bright red fluorescence. Figure 6A–D shows the fluorescence microscopy images of the control, FLS, SLS, and DLS after 24 hours incubation, it was also possible to observe the morphology of fibroblasts, in which all the samples presented green fluorescent staining, without any toxicity. The cytotoxicity of the FLS, SLS, and DLS with respect to the growth of fibroblasts was also analyzed by MTT assay. As illustrated in Figure 6E, although cell viability was inhibited by FLS after 72 hours incubation, the viability of cells treated with the SLS and DLS was not inhibited at all for the predetermined time of incubation. Moreover, chitosan is a natural material that supports cell growth.[46] Therefore, after addition of chitosan to the samples, the scaffolds become more cytocompatible compared with PCL nanofibers. Thus, the prepared DLS wound dressing was considered to be a suitably nontoxic scaffold for wound healing.

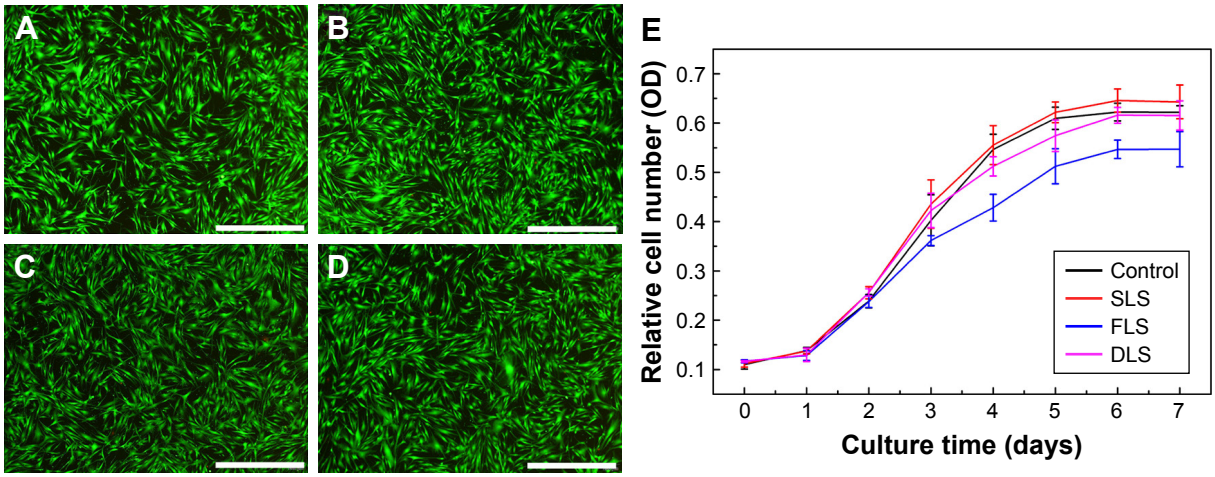

Figure 6 Comparative cytotoxicity of nanofibrous scaffolds.
Notes: Cell viability was determined by live/dead cell assay using calcein-AM (live) and propidium iodide (dead) (**A**–**D**). Representative images of control (**A**), SLS (**B**), FLS (**C**), and DLS (**D**). The viability of human dermal fibroblasts was evaluated using MTT assay (**E**). Scale bar denotes 1 μm.
Abbreviations: DLS, double layer nanofibrous scaffolds; FLS, first layer of scaffolds; SLS, second layer of scaffolds.

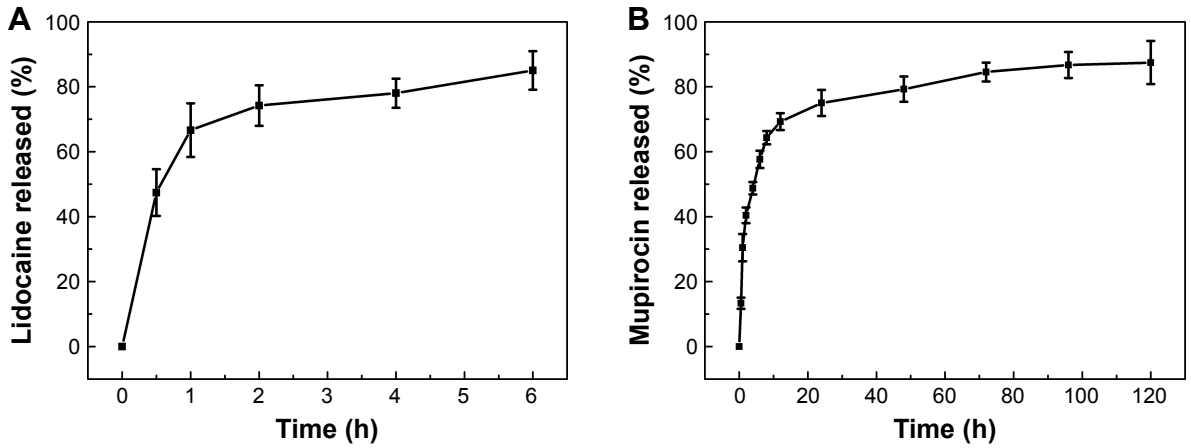

Figure 7 Release profiles of LID and mupirocin into PBS from DLS nanofibrous scaffolds.
Notes: LID eluted from DLS (**A**). Mupirocin eluted from DLS (**B**).
Abbreviations: DLS, double layer nanofibrous scaffolds; LID, lidocaine hydrochloride.

Drug release

Modulation of drug delivery is among the most promising biomedical applications of electrospun materials. Electrospun medicated fibers with a multilayer structure provide multiple opportunities to control release time profiles. The drug release profiles of LID and mupirocin from the DLS are illustrated in Figure 7. The calibration curves of LID at 263 nm and mupirocin at 218 nm were done with $R^2 = 0.9955$ and 0.9984, respectively. LID showed a two-stage release (Figure 7A), with an initial rapid release followed by a slower sustained release. Approximately 66% of LID was released from the DLS in the first hours. The cumulative drug release increased gradually to 85% in the following 6 hours. From a clinical point of view, an initial rapid release in the early stages is beneficial because it helps achieve a therapeutic concentration of the drug in minimal time, followed by sustained release to maintain a minimal effective concentration.[47] Figure 7B shows the results of a prolonged release study of mupirocin from the DLS for 5 days. As is apparent from the figure, the DLS showed a sustained release of mupirocin, similar to the two-stage release profile of LID. The initial rapid release of mupirocin from the DLS resulted in the release of 57% of the total mupirocin content in the first 6 hours. With the sustained release, another 30% was released from the DLS in the following 114 hours. Although similar drug release profiles were observed for LID and mupirocin, 66% of the LID was burst released in the first hour, while only 30% of the mupirocin diffused from the DLS in the same time. This was attributed to the strong chemical linkage interactions of PCL and mupirocin conjugated to the fiber, resulting in a lower release ability of mupirocin compared with LID.

Antibacterial activity

For antimicrobial assessment, the prepared scaffolds were tested against three microorganisms, *S. aureus* (Gram-positive cocci), *E. coli*, and *P. aeruginosa* (Gram-negative rods), using the agar diffusion method to assess their antimicrobial activity. The inhibition zone produced by each sample was measured. Figure 8 shows filter paper control, PCL, FLS, and DLS against *S. aureus*, *P. aeruginosa*, and *E. coli*. Growth of *S. aureus* (18 mm) and *P. aeruginosa* (12 mm) was inhibited by PCL scaffolds. Similar to the control group, the growth of *E. coli* was not inhibited by PCL scaffolds. By contrast, PCL scaffolds loaded on mupirocin showed antibacterial inhibition against all tested microorganisms. The strongest activity was against *S. aureus* (34 mm), followed by *P. aeruginosa* and *E. coli* (31 mm). Mupirocin is an effective antibacterial agent and is often used in clinical practice as topical ointment to treat a wide variety of topical wounds.[8,43] Mupirocin works against a broad spectrum of bacteria by reversibly inhibiting isoleucyl-transfer RNA, thereby inhibiting bacterial protein and RNA synthesis.[48] The DLS showed excellent activity against all tested microorganisms, with the strongest activity against *S. aureus* (35 mm), followed by *P. aeruginosa* (30 mm) and then by *E. coli* (28 mm). Overall, the DLS exhibited significant activity against *S. aureus*, *E. coli*, and *P. aeruginosa*. Therefore, the scaffold developed here could be more effective for treating infected wounds.

Conclusion

In summary, LID and mupirocin were successfully grafted onto a DLS to fabricate a multifunctional scaffold material as a novel wound dressing. The multifunctional scaffolds

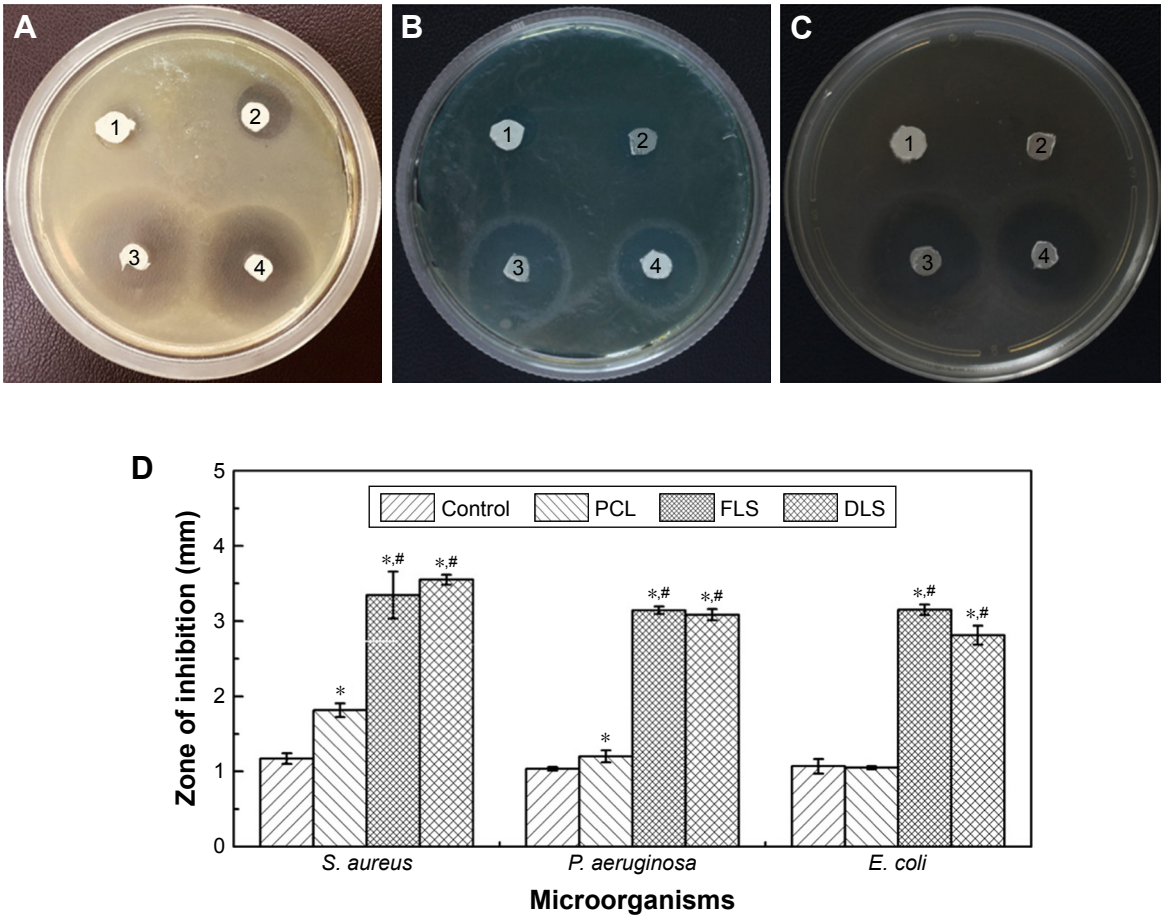

Figure 8 Evaluation of antibacterial activity of nanofibrous scaffolds.
Notes: (1) Filter paper control, (2) PCL, (3) FLS, (4) DLS against *Staphylococcus aureus* (**A**), *Pseudomonas aeruginosa* (**B**), and *Escherichia coli* (**C**) and evaluation of the inhibition zones for filter paper control, PCL, FLS, and DLS against *S. aureus*, *P. aeruginosa*, and *E. coli* (**D**). *The difference in mean is significant ($P<0.05$) with respect to control. #The difference in mean is significant ($P<0.05$) with respect to PCL.
Abbreviations: DLS, double layer nanofibrous scaffolds; FLS, first layer of scaffolds; PCL, polycaprolactone.

displayed optimum porosity and swelling behaviors, which are beneficial for absorbing excess exudates and maintaining a moist environment on the wound surface. Both the tensile strength and Young's modulus of the DLS nanofibers increased dramatically. The DLS was more thermally stable than SLS and FLS. Moreover, the multifunctional DLS showed highly effective antibacterial activities against *S. aureus*, *E. coli*, and *P. aeruginosa* and was nontoxic to fibroblasts. All these results demonstrate that the multifunctional DLS nanofibers have great potential for use as a wound dressing. However, these results need to be substantiated by in vivo studies to further investigate the real-world applications of the scaffold material as a wound dressing.

Acknowledgment

This work was supported by grants from the Chinese Academy of Sciences – Weigao Group High Technology Research and Development Program (ZKYWG2013-05).

Disclosure

The authors report no conflicts of interest in this work.

References

1. Liang D, Lu Z, Yang H, Gao J, Chen R. Novel asymmetric wettable AgNPs/Chitosan wound dressing: in vitro and in vivo evaluation. *ACS Appl Mater Interfaces*. 2016;8(6):3958–3968.
2. Liu M, Luo G, Wang Y, et al. Nano-silver-decorated microfibrous eggshell membrane: processing, cytotoxicity assessment and optimization, antibacterial activity and wound healing. *Sci Rep*. 2017;7(1):436.
3. Mogoşanu GD, Grumezescu AM. Natural and synthetic polymers for wounds and burns dressing. *Int J Pharm*. 2014;463(2):127–136.
4. Chiarini A, Freddi G, Liu D, Armato U, Dal Prà I. Biocompatible silk noil-based three-dimensional carded-needled nonwoven scaffolds guide the engineering of novel skin connective tissue. *Tissue Eng Part A*. 2016;22(15–16):1047–1060.
5. Xu R, Luo G, Xia H, et al. Novel bilayer wound dressing composed of silicone rubber with particular micropores enhanced wound re-epithelialization and contraction. *Biomaterials*. 2015;40:1–11.
6. Metcalfe AD, Ferguson MW. Bioengineering skin using mechanisms of regeneration and repair. *Biomaterials*. 2007;28(34):5100–5113.

7. Ghavaminejad A, Rajan Unnithan A, Ramachandra Kurup Sasikala A, et al. Mussel-inspired electrospun nanofibers functionalized with size-controlled silver nanoparticles for wound dressing application. *ACS Appl Mater Interfaces*. 2015;7(22):12176–12183.
8. Thakur RA, Florek CA, Kohn J, Michniak BB. Electrospun nanofibrous polymeric scaffold with targeted drug release profiles for potential application as wound dressing. *Int J Pharm*. 2008;364(1):87–93.
9. Wu C, Zhang G, Xia T, et al. Bioinspired synthesis of polydopamine/Ag nanocomposite particles with antibacterial activities. *Mater Sci Eng C Mater Biol Appl*. 2015;55:155–165.
10. Chua AW, Khoo YC, Tan BK, Tan KC, Foo CL, Chong SJ. Skin tissue engineering advances in severe burns: review and therapeutic applications. *Burns Trauma*. 2016;4:3.
11. Sultana N, Wang M. Fabrication of HA/PHBV composite scaffolds through the emulsion freezing/freeze-drying process and characterisation of the scaffolds. *J Mater Sci Mater Med*. 2008;19(7):2555–2561.
12. Gao Y, Yang Z, Kuang Y, et al. Enzyme-instructed self-assembly of peptide derivatives to form nanofibers and hydrogels. *Biopolymers*. 2010;94(1):19–31.
13. Sargeant TD, Guler MO, Oppenheimer SM, et al. Hybrid bone implants: self-assembly of peptide amphiphile nanofibers within porous titanium. *Biomaterials*. 2008;29(2):161–171.
14. Gizaw M, Thompson J, Faglie A, Lee SY, Neuenschwander P, Chou SF. Electrospun fibers as a dressing material for drug and biological agent delivery in wound healing applications. *Bioengineering*. 2018;5(1):E9.
15. Ali IH, Khalil IA, El-Sherbiny IM. Single-dose electrospun nanoparticles-in-nanofibers wound dressings with enhanced epithelialization, collagen deposition, and granulation properties. *ACS Appl Mater Interfaces*. 2016;8(23):14453–14469.
16. Ajalloueian F, Tavanai H, Hilborn J, et al. Emulsion electrospinning as an approach to fabricate PLGA/chitosan nanofibers for biomedical applications. *Biomed Res Int*. 2014;2014:475280–13.
17. Abrigo M, McArthur SL, Kingshott P. Electrospun nanofibers as dressings for chronic wound care: advances, challenges, and future prospects. *Macromol Biosci*. 2014;14(6):772–792.
18. Yan S, Li X, Dai J, et al. Electrospinning of PVA/sericin nanofiber and the effect on epithelial-mesenchymal transition of A549 cells. *Mater Sci Eng C Mater Biol Appl*. 2017;79:436–444.
19. Aoki S, Kinoshita M, Miyazaki H, et al. Application of poly-L-lactic acid nanosheet as a material for wound dressing. *Plast Reconstr Surg*. 2013;131(2):236–240.
20. Wang N, Burugapalli K, Wijesuriya S, et al. Electrospun polyurethane-core and gelatin-shell coaxial fibre coatings for miniature implantable biosensors. *Biofabrication*. 2014;6(1):015002.
21. Hu X, Liu S, Zhou G, Huang Y, Xie Z, Jing X. Electrospinning of polymeric nanofibers for drug delivery applications. *J Control Release*. 2014;185:12–21.
22. Hassiba AJ, El Zowalaty ME, Webster TJ, et al. Synthesis, characterization, and antimicrobial properties of novel double layer nanocomposite electrospun fibers for wound dressing applications. *Int J Nanomedicine*. 2017;12:2205–2213.
23. Dang JM, Leong KW. Natural polymers for gene delivery and tissue engineering. *Adv Drug Deliv Rev*. 2006;58(4):487–499.
24. Wang CY, Zhang KH, Fan CY, Mo XM, Ruan HJ, Li FF. Aligned natural-synthetic polyblend nanofibers for peripheral nerve regeneration. *Acta Biomater*. 2011;7(2):634–643.
25. Zine R, Sinha M. Nanofibrous poly(3-hydroxybutyrate-co-3-hydroxyvalerate)/collagen/graphene oxide scaffolds for wound coverage. *Mater Sci Eng C Mater Biol Appl*. 2017;80:129–134.
26. Sadeghi-Avalshahr A, Nokhasteh S, Molavi AM, Khorsand-Ghayeni M, Mahdavi-Shahri M. Synthesis and characterization of collagen/PLGA biodegradable skin scaffold fibers. *Regen Biomater*. 2017;4(5):309–314.
27. Lee KY, Jeong L, Kang YO, Lee SJ, Park WH. Electrospinning of polysaccharides for regenerative medicine. *Adv Drug Deliv Rev*. 2009;61(12):1020–1032.
28. Topuz F, Uyar T. Electrospinning of gelatin with tunable fiber morphology from round to flat/ribbon. *Mater Sci Eng C Mater Biol Appl*. 2017;80:371–378.
29. Noh HK, Lee SW, Kim JM, et al. Electrospinning of chitin nanofibers: degradation behavior and cellular response to normal human keratinocytes and fibroblasts. *Biomaterials*. 2006;27(21):3934–3944.
30. Kishimoto Y, Morikawa H, Yamanaka S, Tamada Y. Electrospinning of silk fibroin from all aqueous solution at low concentration. *Mater Sci Eng C Mater Biol Appl*. 2017;73:498–506.
31. Dongargaonkar AA, Bowlin GL, Yang H. Electrospun blends of gelatin and gelatin-dendrimer conjugates as a wound-dressing and drug-delivery platform. *Biomacromolecules*. 2013;14(11):4038–4045.
32. Ho MH, Yao CJ, Liao MH, Lin PI, Liu SH, Chen RM. Chitosan nanofiber scaffold improves bone healing via stimulating trabecular bone production due to upregulation of the Runx2/osteocalcin/alkaline phosphatase signaling pathway. *Int J Nanomedicine*. 2015;10:5941–5954.
33. Costa-Pinto AR, Reis RL, Neves NM. Scaffolds based bone tissue engineering: the role of chitosan. *Tissue Eng Part B Rev*. 2011;17(5):331–347.
34. Chen ZG, Wang PW, Wei B, Mo XM, Cui FZ. Electrospun collagen-chitosan nanofiber: a biomimetic extracellular matrix for endothelial cell and smooth muscle cell. *Acta Biomater*. 2010;6(2):372–382.
35. Zuo PP, Feng HF, Xu ZZ, et al. Fabrication of biocompatible and mechanically reinforced graphene oxide-chitosan nanocomposite films. *Chem Cent J*. 2013;7(1):39.
36. Fu W, Liu Z, Feng B, et al. Electrospun gelatin/PCL and collagen/PLCL scaffolds for vascular tissue engineering. *Int J Nanomedicine*. 2014;9:2335–2344.
37. Chen H, Fan X, Xia J, et al. Electrospun chitosan-graft-poly (ε-caprolactone)/poly (ε-caprolactone) nanofibrous scaffolds for retinal tissue engineering. *Int J Nanomedicine*. 2011;6:453–461.
38. Zhou T, Sui B, Mo X, Sun J. Multifunctional and biomimetic fish collagen/bioactive glass nanofibers: fabrication, antibacterial activity and inducing skin regeneration in vitro and in vivo. *Int J Nanomedicine*. 2017;12:3495–3507.
39. Alhosseini SN, Moztarzadeh F, Mozafari M, et al. Synthesis and characterization of electrospun polyvinyl alcohol nanofibrous scaffolds modified by blending with chitosan for neural tissue engineering. *Int J Nanomedicine*. 2012;7:25–34.
40. Frohbergh ME, Katsman A, Botta GP, et al. Electrospun hydroxyapatite-containing chitosan nanofibers crosslinked with genipin for bone tissue engineering. *Biomaterials*. 2012;33(36):9167–9178.
41. Soliman S, Sant S, Nichol JW, Khabiry M, Traversa E, Khademhosseini A. Controlling the porosity of fibrous scaffolds by modulating the fiber diameter and packing density. *J Biomed Mater Res A*. 2011;96(3):566–574.
42. Wei Y, Nedley MP, Bhaduri SB, Bredzinski X, Boddu SH. Masking the bitter taste of injectable lidocaine HCl formulation for dental procedures. *AAPS Pharm Sci Tech*. 2015;16(2):455–465.
43. Perumal S, Ramadass S, Madhan B. Sol-gel processed mupirocin silica microspheres loaded collagen scaffold: a synergistic bio-composite for wound healing. *Eur J Pharm Sci*. 2014;52:26–33.
44. Sailakshmi G, Mitra T, Gnanamani A. Engineering of chitosan and collagen macromolecules using sebacic acid for clinical applications. *Prog Biomater*. 2013;2(1):11.
45. Ye S, Jiang L, Wu J, et al. Flexible amoxicillin-grafted bacterial cellulose sponges for wound dressing: in vitro and in vivo evaluation. *ACS Appl Mater Interfaces*. 2018;10(6):5862–5870.
46. Regiel-Futyra A, Kus-Liśkiewicz M, Sebastian V, et al. Development of noncytotoxic chitosan-gold nanocomposites as efficient antibacterial materials. *ACS Appl Mater Interfaces*. 2015;7(2):1087–1099.
47. Shi S, Zhang Z, Luo Z, et al. Chitosan grafted methoxy poly(ethylene glycol)-poly(ε-caprolactone) nanosuspension for ocular delivery of hydrophobic diclofenac. *Sci Rep*. 2015;5:11337.
48. Dürrigl M, Kregar ML, Hafner A, Klarić MŠ, Filipović-Grčić J. Mupirocin calcium microencapsulation via spray drying: feed solvent influence on microparticle properties, stability and antimicrobial activity. *Drug Dev Ind Pharm*. 2011;37(12):1402–1414.